



Simulation of compressive strength of wall studs cold-formed from advanced high strength steels

Chu Ding¹, Yu Xia², Damir Akchurin³, Zhanjie Li⁴, Hannah Blum⁵, Benjamin W. Schafer⁶

Abstract

The objective of this paper is to explore if the structural design of thin-walled cold-formed steel wall studs constructed from advanced high strength steels (AHSS), with yield stress which may exceed 1000 MPa (145 ksi), require modifications relative to the design provisions for conventional cold-formed steel. A computational-based parametric study is explored utilizing shell finite element collapse analyses. The parametric study covers three steel materials, two AHSS and one mild steel, which are all 152 mm (6 in.) deep commercial structural lipped channels listed by the Steel Framing Industry Association (SFIA) and involves two bracing configurations which simulate real bracing conditions commonly found in cold-formed steel building applications. The simulated strengths from the finite element models are compared to the predictions by the Direct Strength Method (DSM) in the North American cold-formed steel specification AISI S100-16. Modal identification techniques are also applied to the simulation results to quantify the existence and importance of local-distortional and distortional-global buckling mode interactions, and to explore their implications on the strength predictions. It is shown that for practical cross-sections and bracing conditions, the current Direct Strength Method expressions can accurately predict the compressive strengths of the simulated AHSS walls studs. However, it is shown that the shape of the material stress-strain response in addition to yield stress does have an impact on the results and further examination of modal interactions is still underway. This study marks one of the initial steps towards making AHSS available for use in the cold-formed steel construction industry.

1. Introduction

As the outcome of more than two decades of research and development in material science, advanced high strength (AHSS) refers to a group of new sheet steel grades with unique

¹ Graduate Research Assistant, Department of Civil & System Engineering, Johns Hopkins University, chud@jhu.edu

² Graduate Research Assistant, Department of Civil & Environmental Engineering, University of Wisconsin-Madison, yxia44@wisc.edu

³ Graduate Research Assistant, Department of Civil & System Engineering, Johns Hopkins University; former undergraduate research assistant at SUNY Polytechnic Institute, akchurd1@jhu.edu

⁴ Associate Professor of Civil Engineering, SUNY Polytechnic Institute, liz1@sunypoly.edu

⁵ Assistant Professor, Department of Civil & Environmental Engineering, University of Wisconsin-Madison, hannah.blum@wisc.edu

⁶ Professor, Department of Civil & Environmental Engineering, Johns Hopkins University, schaffer@jhu.edu

combinations of strength and ductility. At this moment, over 20 steel grades exist under the name of AHSS. These steel grades vary in strength and ductility and greatly expand the strength and ductility potential beyond the traditional mild and high-strength low alloy (HSLA) steels. Among AHSS include dual-phase (DP) and martensitic (MS) steels which are prime candidates to be adopted as next-generation cold-formed construction steel, not only for their superior strength (beyond 1000 MPa yield strength) and but also potential affordability. At this moment, none of the AHSS grades are adopted in national design specifications such as AISI S100 (2016). Research on the structural behavior of the members cold-formed from AHSS is specially needed for AHSS to be adopted for cold-formed steel (CFS) construction usage.

Higher slenderness of AHSS members can be a challenge to the current design specification. For example, a cold-formed steel member formed from a 145 ksi (1000 MPa) AHSS grade will have slenderness 1.7 times that of a member formed from a typical 50 ksi (345 MPa) mild steel. The current design method, e.g., the Direct Strength Method (DSM) in AISI S100, which has been used widely for strength prediction and shape optimization (Leng et al. 2014; Li et al. 2016), is an empirical method based on experimental and numerical data which consist of members of largely low to medium slenderness and limited data of high slenderness (Camotim et al. 2016; Schafer 2008, 2019). The higher slenderness of AHSS members will push the current design strength method to the boundaries where the underpinning data is relatively scarce. Additionally, there is potential for more mode interactions for CFS members with high slenderness. At higher slenderness, there is more deformation prior to peak strength for the different buckling modes to interact with each other potentially leading to strength erosion. Significant work on the mode interaction has been carried out and multiple proposals been made to address them (Chen et al. 2020; Dias Martins et al. 2017; Dinis et al. 2018, 2020; Martins et al. 2015, 2018; Silvestre et al. 2012). In the early development of the DSM, the limit states of various mode interactions (LG, DL, DG and LDG) were also considered, where G = global, D = distortional, and L = local. However, only the limit state of LG interaction was kept because the inclusion of the remainder was found to be overly conservative (Schafer 2002). With the current DSM only considering LG interaction, it is worth investigating whether other types of interactions will appear more prevalent in AHSS members and potentially reduce the accuracy of the DSM.

High slenderness is not the only change that AHSS creates. The constitutive behavior, specifically stress-strain curves of AHSS are also different from those of the mild steel. The typical constitutive behavior of mild cold-formed steel used in the North America has a short but clear yield plateau and abundant ductility. The AHSS grades, however, typically do not have clear yield plateaus (Xia et al. 2021) and often possess limited ductility, especially for the grades on the upper side of the strength spectrum such as martensitic (MS) steels. The strength in the local and distortional buckling limit states come from post-buckling reserve of the cross sections which for large ranges of slenderness does have an inelastic contribution. It is an open question as to whether such difference in inelasticity will affect the DSM's effectiveness in predicting the strengths of AHSS members.

It is these unique characteristics of AHSS that prompt this research on the compressive strengths of AHSS cold-formed members. Many numerical studies on cold-formed steel compression members have been conducted in the past, which largely focus on cold-formed steel members under perfect idealized boundary conditions and loading. Though very useful in understanding

buckling behaviors, these types of simulations may not represent the real-world working conditions of cold-formed steel compression members, particularly due to their lack of consideration for bracing. Bracing common in wall applications such as bridging and sheathing can significantly influence the buckling modes and may affect buckling mode interactions. To advance knowledge of the strengths of the cold-formed steel members in real-world conditions, this study investigates the compressive strengths of AHSS members in the context of cold-formed steel gravity wall studs, a type of compression member ubiquitous in the cold-formed steel structures. It is believed that this study will contribute to bringing AHSS into the realm of cold-formed steel construction.

2. Numerical Parametric Study

This section presents a large numerical parametric study into the compressive strengths of AHSS members in the context of cold-formed steel gravity wall studs.

2.1 Simulation Matrix

The simulation matrix of the parametric study is developed based on three parameters: cross section, stud bracing, and materials. The build-up of the simulation matrix is shown in Figure 1. The cross section includes all the 6 in. (152 mm) deep lipped channel sections commercially available in the SFIA catalog (SFIA 2018), in total 26 cross sections. The selection of 6 in. (152 mm) deep cross section is representative of the wall thickness typically used in the United States.

Two types of column bracings are considered: discrete bracing and combined bracing. Discrete bracing refers to the case in which the wall stud is bracing by a discrete steel bridging channel. Combined bracing refers to the case in which both bridging channel and wall sheathing contribute to stud bracing. The combined bracing case is the most realistic case for final as-built conditions of the wall studs in practice, while the discrete bracing exists in the construction phase before the wall sheathing is installed and is often assumed as the only bracing present by structural engineers for design simplicity and safety.

One of the key focuses of this study is the material influence. Three representative steel types are considered: 50 ksi (345 MPa) nominal yield mild steel, 101 ksi (700 MPa) nominal yield dual-phase steel - DP700, and 174 ksi (1200 MPa) nominal yield martensitic steel - MS1200. The total number of simulation models in this study is 26 (cross sections) x 2 (bracing conditions) x 3 (materials) = 156 models.

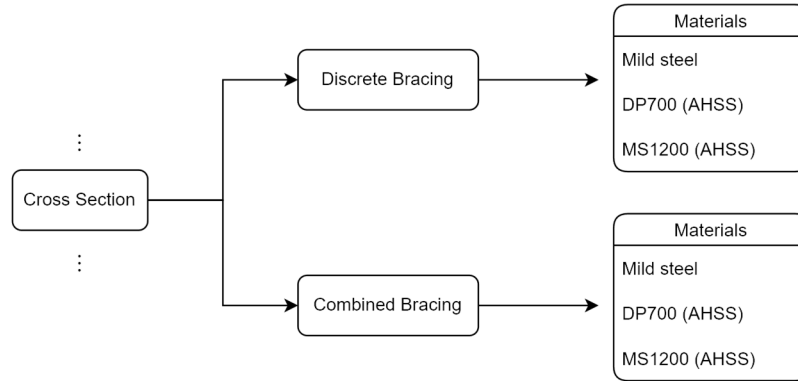


Figure 1: Simulation matrix

2.2 Finite Element Model

The numerical parametric study is conducted through finite element analysis in Abaqus Standard (2016). The finite element model is shown in Figure 2. The cold-formed steel lipped channel is modeled by the 8-node shell element S8R. A fixed-fixed boundary condition (consistent with a stud in track under sustained dead load) is assumed at each end. The model is loaded through the imposed displacement in the Y direction at one end of the wall stud as shown in . To facilitate the creation of the boundary conditions, each end of the wall stud is assigned rigid body constraint (PIN) to a reference node. The boundary condition is imposed through the reference nodes.

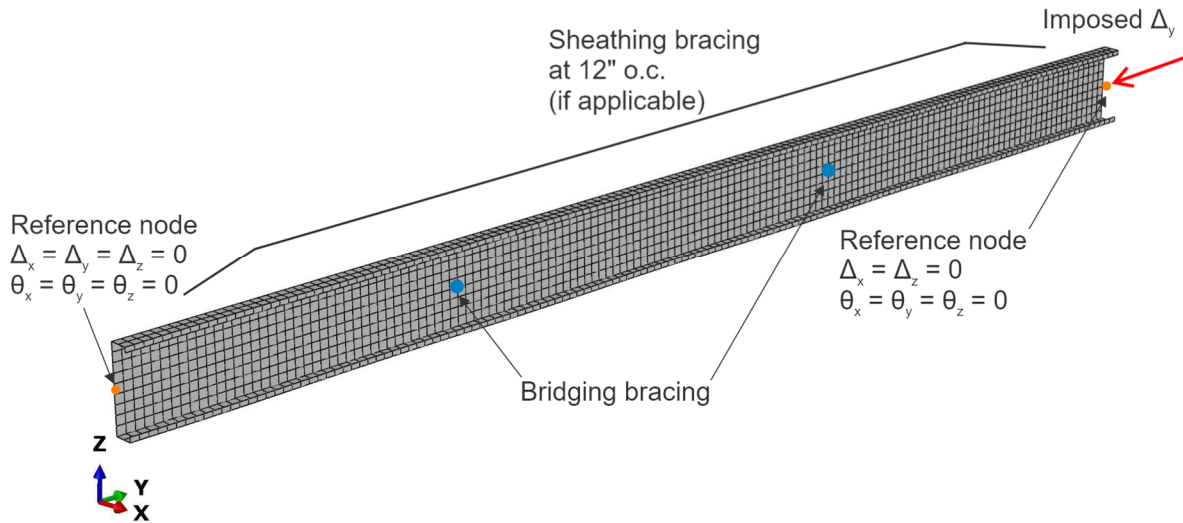


Figure 2: Finite element model of the AHSS wall studs

Two types of real-life bracing conditions as discussed earlier in this section, discrete bracing, and combined bracing, are simulated in the finite element models. To consider bridging bracing, bracing is modeled at the third points of the studs. For sheathing bracing, bracing is modeled at 12” on center along the member length connected to the flanges. Both bracings are modeled as springs. The details of the spring arrangement and stiffness are discussed in the next section.

2.3 Bracing Models

Bridging restrains both the lateral movement and torsion of the wall studs. A group of ground springs, including one axial spring and one rotational spring, is used to model this restraint, as shown in Figure 3 (a). Through screwed connections and the contact with the web of the stud, bridging exerts restraint over a portion of the web instead of at one point. To simulate this effect, a portion of the stud web is assigned with a rigid body constraint by a reference node, and the group of the springs is directly assigned to the reference node. The extent of the rigid body constraint is set to be between the two screw connections, each of which is 3/4 in. (19 mm) from the end of the web. The distance of 3/4 in. (19 mm) is based on an assumed 1/2 in. (13 mm) end distance screw connection and 5-1/2 in. (152 mm) width for the clip angle.

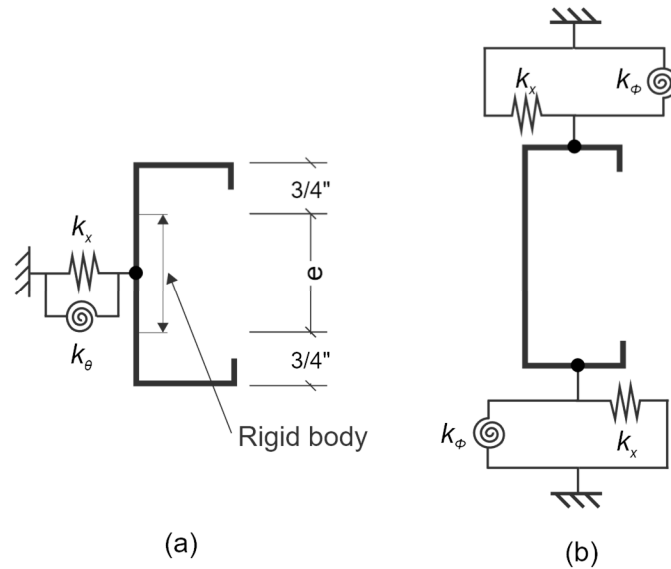


Figure 3: Bracing model (a) bracing by bridging (b) bracing by sheathing

The stiffness of bridging bracing depends on the whole bridging system. The bridging system typically consists of a clip angle and a U channel. The axial and flexural rigidity of the U channel is applied to the wall stud through the clip angle which screw fastened to the web of the wall stud. This parametric study considers a short gravity wall for which the clip angle stiffness controls the overall bridging bracing stiffness. For simplicity, the bridging stiffness is set to be the clip angle stiffness. The clip angle stiffnesses as tabulated in Table 1 are referenced from the study by Urala (2004) which tested the bridging connections at various configurations. For configurations not covered by Table 1, bilinear interpolation is applied to get the estimated stiffness.

Table 1: Bridging clip angle stiffness*

	Axial stiffness (kip/in.)				Torsional stiffness (kip·in./rad)			
	33 mil	43 mil	68 mil	97 mil	33 mil	43 mil	68 mil	97 mil
H = 3.625 in.	1.88	3.89	7.02	\	3.48	6.19	14.80	\
H = 6.000 in.	1.07	3.80	\	4.72	7.11	22.56	\	37.49
H = 8.000 in.	\	2.27	\	5.02	\	55.87	\	74.64

* Value referenced from Urala (2004)

Sheathing bracing, which is provided through the sheathing-to-steel connections over the top and bottom flanges of the studs, is also simulated by a group of axial and rotational springs. The sheathing bracing provides both the lateral and the rotational restraint at each flange. In this parametric study, all wall studs are spaced at 16" in. on center and are sheathed with 7/16 in. (11 mm) thick gypsum board with #6 screw of 5/32 in. (4.0 mm) nominal diameter at 12 in. on center. The stiffnesses of the springs are calculated based on the predictive equations proposed by Vieira and Schafer (2013). The results are shown in Table 2.

Table 2: Sheathing bracing stiffness

Thickness	Lateral stiffness	Rotational stiffness
	k_x (kip/in.)	k_θ (kip·in./rad)
33 mil	0.38	0.72
43 mil	0.78	0.77
54 mil	1.37	0.84
68 mil	2.22	0.93
97 mil	3.76	1.15
118 mil	4.49	1.31

1 kip/in. = 175.1 N/mm; 1 kip·in./rad = 112,979.2 N·mm/rad

2.4 Material Models

Material influence is one of the key focuses of this study. To achieve reasonable representation of the behaviors of each material, generic material constitutive models are synthesized from a database of CFS materials which contain over 400 coupon test curves of various mild steel and AHSS ("CFS Material Database" 2021).

For the mild cold-formed steel, a Ramberg-Osgood based material model (Yun and Gardner 2017) as shown in Eq. (1), initially developed for hot rolled steel with long yield plateau, is adopted for synthesizing generic mild cold-formed steel stress-strain curves. It is found that this material model is generally applicable to mild cold-formed steel if correct ϵ_{sh} and ϵ_u are provided. Using the 196 mild cold-formed steel coupon data, the key inputs ϵ_{sh} and ϵ_u are summarized in Table 3 based on the nominal yield strength. The generic mild CFS stress-strain curves are synthesized by applying the mean parameters to the corresponding mild CFS material model.

$$F(\epsilon) = \begin{cases} E\epsilon & \text{for } \epsilon \leq \epsilon_y \\ F_y & \text{for } \epsilon_y < \epsilon \leq \epsilon_{sh} \\ F_y + (F_u - F_y) \left\{ 0.4 \left(\frac{\epsilon - \epsilon_{sh}}{\epsilon_u - \epsilon_{sh}} \right) + 2 \left(\frac{\epsilon - \epsilon_{sh}}{\epsilon_u - \epsilon_{sh}} \right) / \left[1 + 400 \left(\frac{\epsilon - \epsilon_{sh}}{\epsilon_u - \epsilon_{sh}} \right)^5 \right]^{1/5} \right\} & \text{for } \epsilon_{sh} < \epsilon \leq \epsilon_u \end{cases} \quad (1)$$

Table 3: Constitutive model parameters of the mild steel (MPa = 6.895×ksi)

Material	Statistics	F_y (ksi)	F_u (ksi)	ϵ_{sh}	ϵ_u
Nominal yield 33 ksi*	Mean	49.68	59.63	0.03	0.20
	SD	11.35	10.13	0.01	0.04
	COV	0.23	0.17	0.45	0.22
Nominal yield 50 ksi	Mean	52.52	68.84	0.01	0.16
	SD	6.14	8.33	0.01	0.03
	COV	0.12	0.12	0.72	0.21
Nominal yield 60 ksi	Mean	78.86	84.31	0.02	0.11
	SD	0.15	0.04	0.004	0.04
	COV	0.002	0.001	0.17	0.32

* it is common to provide 50 ksi or near 50 ksi material when 33 ksi is specified

For the AHSS materials, work has already been completed, in which stress-strain curves obtained from AHSS coupon tests are fit to a modified Ramberg-Osgood material model (Xia et al. 2021). The statistical mean values of the fitted parameters are selected to produce the generic constitutive material model, for both DP700 and MS1200 steels.

The three generic material engineering stress-strain curves (mild, DP700 and MS1200) are shown in Figure 4. The mild steel stress-strain curve possesses a short yield plateau which does not exist among DP700 and MS1200 materials. Additionally, both DP700 and MS1200 have limited strain hardening phase while the mild steel has long strain hardening phase.

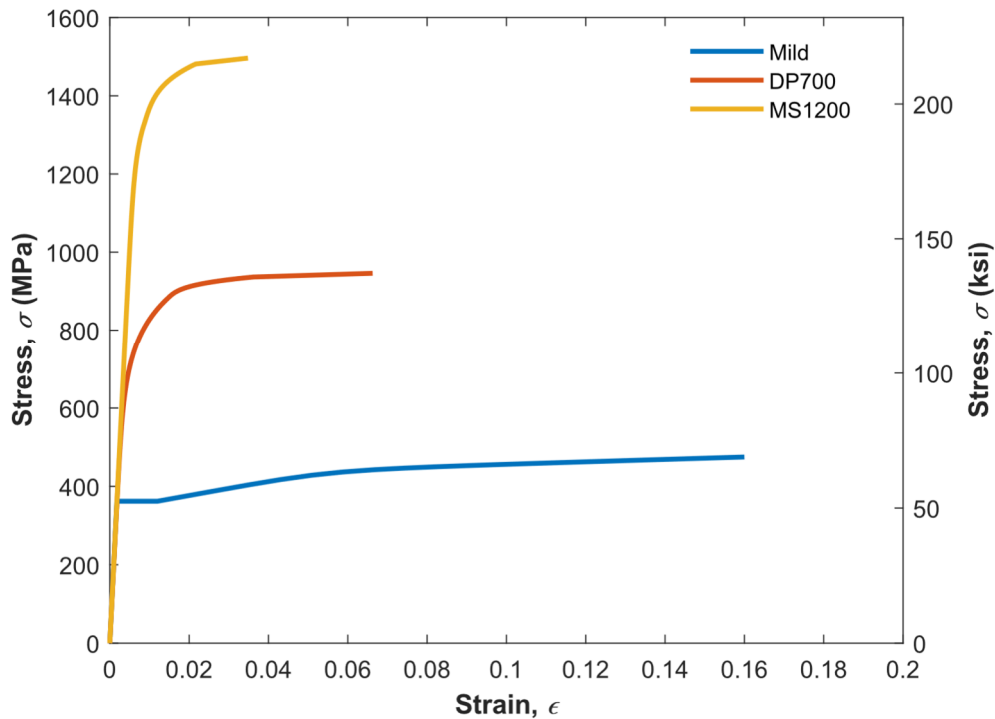


Figure 4: Engineering stress-strain curves of the generic materials

The obtained generic material stress-strain curves are discretized to be consistent with the elastic-plastic material model configuration in Abaqus. Linear elasticity with Young's modulus of 295,000 ksi (203,400 MPa) is assumed in the material model before stress reaches yield stress F_y or $F_{y,0.2}$ (0.2% offset stress). Beyond yielding or 0.2% offset stress, a plastic model is assumed, which is implemented by sampling from the portion of the generic material curves where stress exceeds F_y or $F_{y,0.2}$. The plastic material models for the three materials are shown in Figure 5. It is worth noting that the synthesized generic material curves are engineering values, therefore conversion to true stress-strain values were performed before being used in the Abaqus material model.

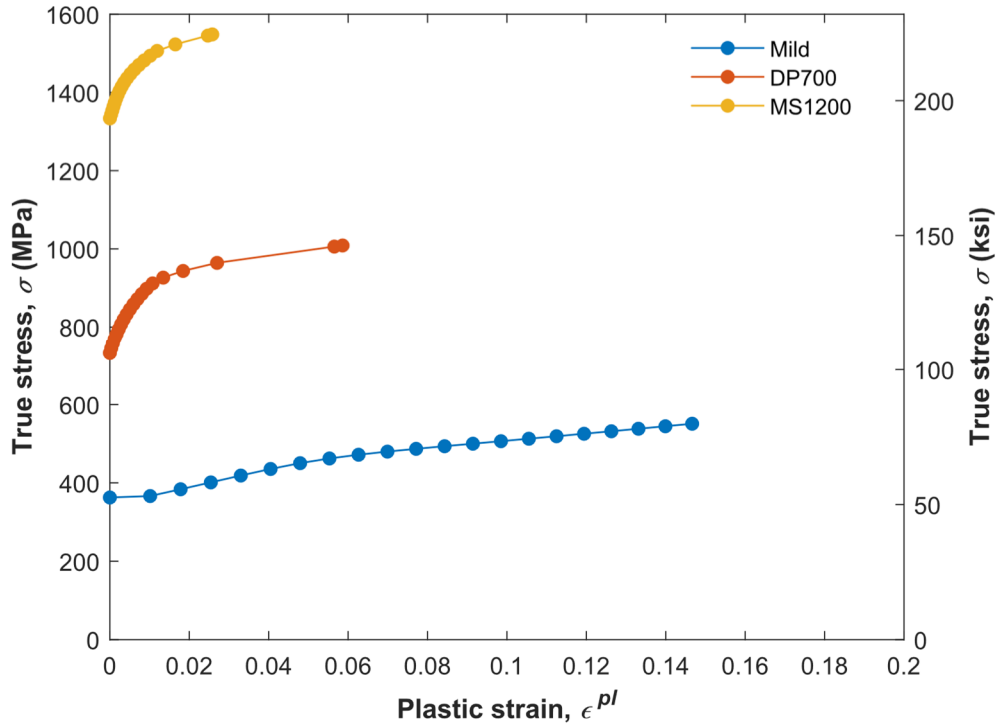


Figure 5: Plastic material models of mild, DP700 and MS1200

2.4 Imperfections

Geometric imperfections are applied through superimposing elastic buckling modes on the undeformed geometry. The imperfections applied include three global modes (bow, camber, twist) and two local modes (type 1 and type 2) as introduced by (Schafer and Peköz 1998). The imperfection magnitudes are based on a statistical summary on imperfection by (Zeinoddini and Schafer 2012), which is summarized in Table 4. The 50%ile magnitudes are selected for this study.

Table 4: Imperfection ratios by statistical percentiles

Magnitude	Global imperfection			Local imperfection	
	Bow	Camber	Twist	Type 1	Type 2
	L / δ_b	L / δ_c	deg. / ft.	d_1 / t	d_2 / t
25%ile	5963	957	0.03	0.17	0.43
50%ile	3248	5452	0.06	0.31	0.75
75%ile	1717	3523	0.12	0.54	1.14
95%ile	865	1582	0.25	1.02	3.06
99%ile	740	1284	0.25	3.87	4.46

L = length, t = thickness, δ_b = bow imperfection, δ_c = camber imperfection, d_1 = type 1 imperfection, d_2 = type 2 imperfection

3. Simulation Results Compared to Code DSM Predictions

The wall stud strengths obtained from all 156 simulations are compared with the strength predictions by the direct strength method (DSM) per AISI S100 (2016). The peak compressive loads in the finite element analysis are taken as the ultimate strengths P_u of the simulated wall studs. For the DSM predictions, the predicted strengths are taken as the minimum of the three limit state nominal strengths, yielding or global buckling P_{ne} , local buckling interacting with global buckling P_{nl} , and distortional buckling P_{nd} .

The key input to the DSM limit state strength prediction are the elastic critical buckling loads: critical global buckling P_{cre} , critical local buckling P_{crl} and critical distortional buckling P_{cra} . These elastic buckling loads are determined from the finite strip analysis whose boundary conditions and bracing restraints are consistent with the corresponding finite element models. Finite strip modal identification is implemented in each analysis and a 50% exceedance rule for modal participation is used to select the critical buckling modes. The consideration of the bracing conditions has minor increase on the critical local buckling loads, but larger boosts for the critical distortional buckling, with a 24% average increase for the combined bracing case and a 3% average increase for the discrete bracing case, where the increases are over the bare section results determined through the conventional two-step method (Li and Schafer 2010).

The results of the 156 finite element models are plotted against DSM design curves in the format of slenderness vs normalized strength in Figure 6, with each data point representing one finite element analysis. It is worth noting that the data are only plotted against their dominant limit state as predicted by the DSM. As shown in Figure 6, the vast majority of the simulations are predicted by the DSM to be dominated by the local-global limit state. The DSM design curves are found to generally follow the simulation results.

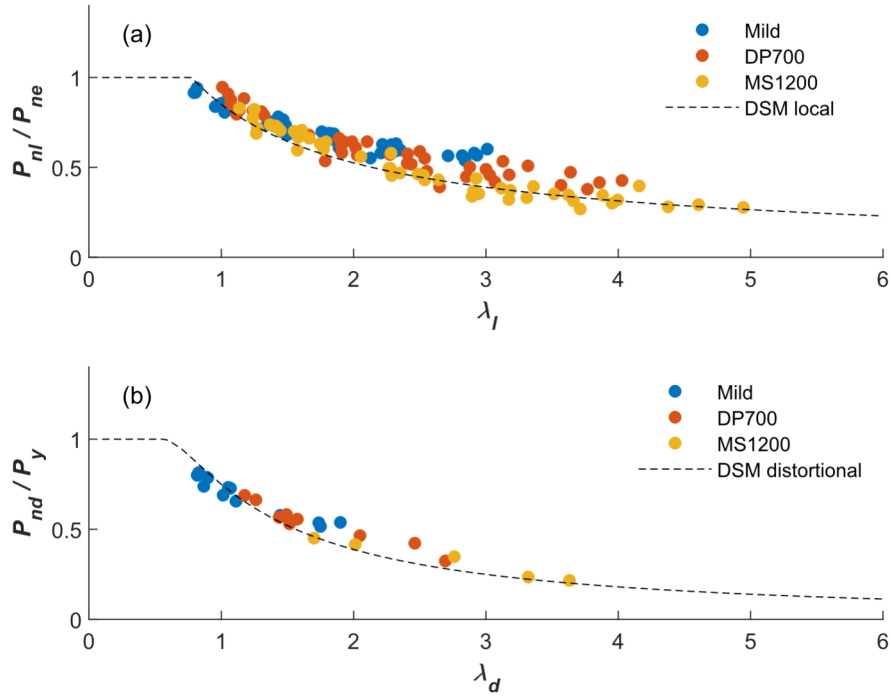


Figure 6: Simulation strength versus code DSM prediction (a) local buckling dominant (b) distortional buckling dominant

The simulation-to-predicted ratios P_u/P_n are summarized in Table 5. Overall, the DSM provides reasonably accurate strength predictions for the finite element wall stud models considered in this parametric study, with the mean P_u/P_n ratio equal to 1.12 for all materials. Though all the strength predictions are conservative, the predictions for MS1200 are less conservative than those for the mild steel and DP700, with the mean P_u/P_n ratio equal to 1.03 for all modes while the ratios of the other two materials are 1.13 and 1.16.

Table 5: Simulation-to-predicted ratios

Material	Statistics	Simulation-to-predicted ratios		
		Local-Global	Distortional	All modes
Mild	Mean	1.17	1.03	1.13
	COV	0.13	0.12	0.14
DP700	Mean	1.17	1.13	1.16
	COV	0.10	0.09	0.10
MS1200	Mean	1.03	1.09	1.03
	COV	0.09	0.10	0.09
All materials	Mean	1.12	1.07	1.11
	COV	0.12	0.11	0.12

4. Effect of Mode Interactions

The high slenderness of AHSS members allow for larger elastic deformation and greater potential for mode interactions to develop, which may potentially lead to strength erosion. This section examines the effect of the mode interaction from the simulation data reported in this parametric

study. Currently, the DSM in AISI S100 only considers local-global interaction. Other mode interactions, namely local-distortional and distortional-global as well as local-distortional-global interactions, are not considered based on the studies by Schafer (2002). This discussion focuses on these additional mode interactions not considered by the DSM in AISI S100.

For local-distortional interaction, a key indicator from the literature (Dias Martins et al. 2017) is the ratio of the critical distortional buckling load to the critical local buckling load P_{crd}/P_{crl} . The ratio P_{crd}/P_{crl} divides the local-distortional interaction into three types: true distortional (D) + local (L), secondary distortional (D) interaction, secondary local (L) interaction. Among the three types of interaction, the true D+L interaction has the largest strength erosion, and the secondary D interaction has the second largest. Since the current DSM does not consider local-distortional limit state, for the simulations experiencing pure D+L interaction, it is expected to have lower simulation-to-predicted ratios P_u/P_n . This method is implemented in Figure 7 (a), with the P_u/P_n ratios plotted against the P_{crd}/P_{crl} ratios. As shown in Figure 7 (a), the simulation data reported in this study can be divided into two categories, with one group predicted to experience true D+L interaction and the other predicted to experience secondary D interaction. However, the simulation-to-predicted ratios P_u/P_n of the simulation results in this study do not display a strong correlation with P_{crd}/P_{crl} ratio. The simulations characterized as pure D+L interaction are found to have slightly less conservative prediction (mean $P_u/P_n = 1.07$) than those characterized as secondary D interaction (mean $P_u/P_n = 1.14$), indicating potentially minor strength erosion caused by local-distortional interaction. In comparison to past work, these simulations are braced, and this is reflected in the elastic buckling loads. It is hypothesized that the presence of the elastic bracing changes the nature of the interactions observed in the work of others on bare, unbraced sections.

The effect of potential distortional-global interaction is also studied. The global to distortional critical buckling ratio P_{cre}/P_{crd} is proposed by Martins et al. (2018) to predict the tendency for the distortional-global interaction, which also divides interaction into three types: pure distortional-global interaction when $P_{cre}/P_{crd} \approx 1.0$, secondary distortional (D) or global (G) when P_{cre}/P_{crd} is larger or smaller than 1.0. The members with P_{cre}/P_{crd} closer to 1.0 are expected to experience larger strength erosion caused by the distortional-global interaction. The simulation-to-predicted ratios P_u/P_n of this study versus P_{cre}/P_{crd} are shown in Figure 7 (b). Overall, the simulation-to-predicted ratio P_u/P_n does not show strong correlation with the ratio of global to local critical buckling ratio P_{cre}/P_{crd} . However, it can be observed that the simulation data with P_{cre}/P_{crd} smaller than 4.5 have lower P_u/P_n ratios (mean $P_u/P_n = 1.05$) than those with P_{cre}/P_{crd} larger than 4.5 (mean $P_u/P_n = 1.16$), which indicates slight strength erosion due to distortional-global interaction.

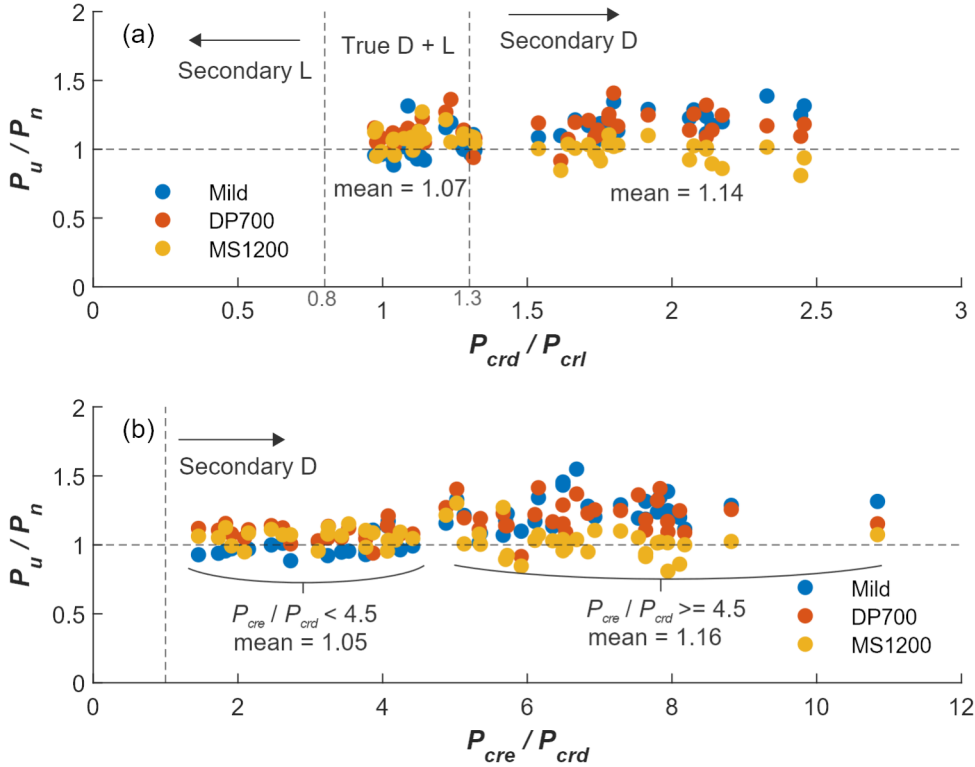


Figure 7: Potential effect of mode interactions on strength by ratios of elastic critical buckling loads (a) D+L interaction (b) D+G interaction

The modal identification method developed by Li et al. (2013) allows decomposing finite element model deformed shapes into deformation modes with corresponding participation percentages. The deformation modes include three buckling modes, which are global buckling (G), distortional buckling (D), local buckling (L), and one shear or transverse extension mode (ST). The modal identification method is applied over all the simulation models in this study. The participation percentages for the three buckling modes determined through this analysis and labeled as such, Γ_G for G mode, Γ_D for D mode and Γ_L for L mode. The participation percentages at the 85% peak load levels are shown in Figure 8. Although the current DSM predicts that most simulation models fail in the local-global buckling limit state, the modal identification shows D mode as the most dominant mode by participation percentages. Among the three materials considered, AHSS materials are found to have higher D mode participation and lower L mode and G mode participations than the mild steel. From the perspective of DSM predictions, higher D mode participation is not found to coincide with lower simulation-to-predicted ratios for all three materials. This finding suggests that the L-G DSM curve may be overly conservative, and it is found that the L-G strength and D strength are very close to one another in many of the simulated cases.

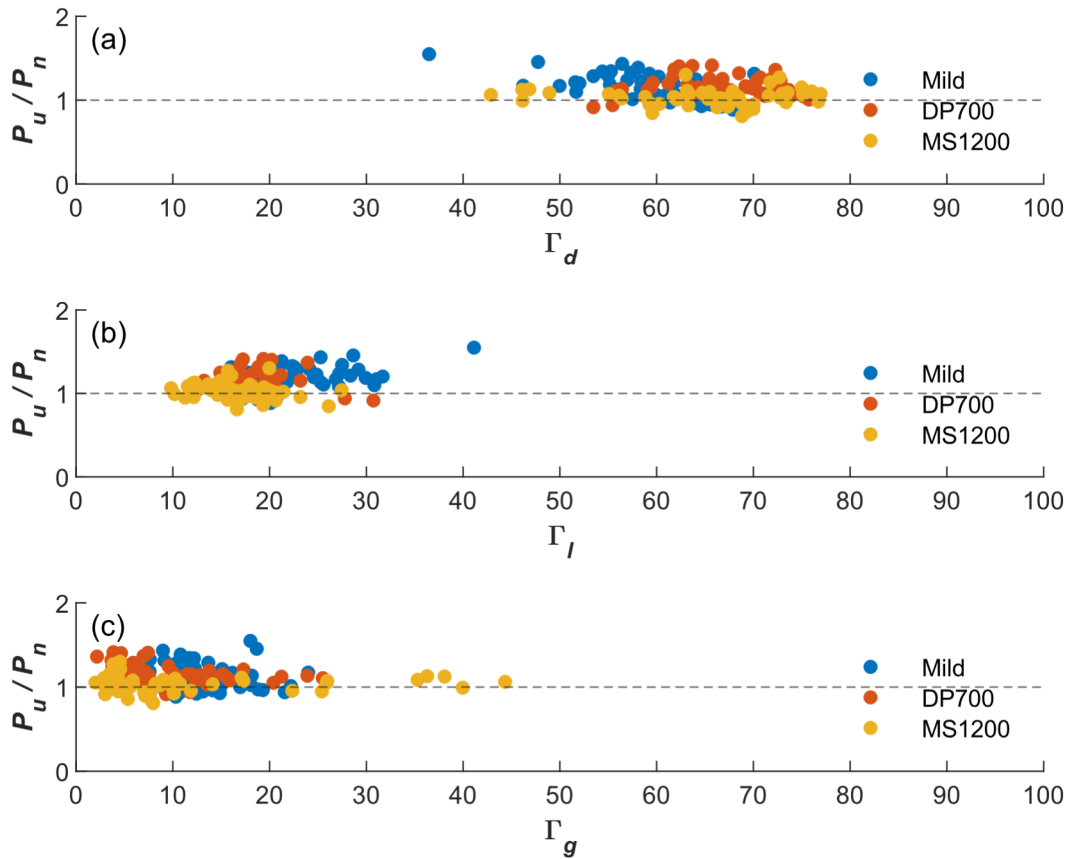


Figure 8: Effect of mode of interactions on strength by modal participation (a) distortional participation (b) local participation (c) global participation

Discussion

This paper presents a parametric numerical study which is largely based on real-life boundary and bracing conditions of cold-formed steel compression members. The authors hypothesize that the realistic bracing conditions considered in this study (bridging and sheathing) greatly contribute to the strength of the simulated members through significantly increasing distortional buckling strength and limiting the potential development of mode interactions. It is believed that the inclusion of expected bracing conditions makes the simulation data of this study a distinct addition to the earlier simulation study based on models without bracings. Although DSM is found to provide an adequate strength prediction for AHSS steels, it is also found that the higher strength MS steels are the least conservative, and additionally that the dominant predicted limit state by DSM (L-G) is not always consistent with observations that suggest D should control most of the failures.

4. Conclusions

This paper presents a parametric numerical study on the compressive strengths of structural lipped channels cold-formed from advanced high strength steel (AHSS) and utilized in the context of typical gravity wall studs. The realistic conditions for the typical gravity wall studs are achieved

in the finite element modeling by simulating the steel bridging and sheathing bracing condition by spring elements. The simulation results are compared to the strength predictions for the Direct Strength Method (DSM) as implemented in AISI S100, which finds that the current DSM is capable of accurately predicting the compressive strengths of the AHSS members under discrete and combined bracing conditions. The mode interaction effect is also explored with the help of both the critical buckling ratio method and the modal identification method. The examination of the simulations conducted in this study does not lead to evidence of worse performance of code predictions due to potential mode interactions, but further study may be warranted particularly because of the relative consistency between the DSM and the deformation-based modal identification in predicting the dominant limit state. Overall, this study advances the understanding of the current specification's applicability to new AHSS steel grades.

Acknowledgments

This paper is based upon work supported by the U.S. National Science Foundation under Grant No. 1760953. Any opinions, findings, and conclusions or recommendations expressed in this material are those of the author(s) and do not necessarily reflect the views of the National Science Foundation.

References

- “Abaqus Standard.” 2016. *Dassault Systemes Simulia Corporation, Providence, RI, USA.*
- AISI S100. 2016. *North American Specification for the Design of Cold-Formed Steel Structural Members.* AISI S100-16, American Iron and Steel Institute, Washington, DC.
- Camotim, D., Dinis, P. B., and Martins, A. D. 2016. “4 - Direct strength method—a general approach for the design of cold-formed steel structures.” *Recent Trends in Cold-Formed Steel Construction*, C. Yu, ed., Woodhead Publishing, 69–105.
<https://doi.org/10.1016/B978-0-08-100160-8.00004-9>.
- “CFS Material Database.” 2021. *Next Generation Construction Steel Project*, <<https://cfs-database.com/>><https://cfs-database.com/>.
- Chen, M.-T., Young, B., Martins, A. D., Camotim, D., and Dinis, P. B. 2020. “Experimental investigation on cold-formed steel stiffened lipped channel columns undergoing local-distortional interaction.” *Thin-Walled Structures*, 150, 106682.
<https://doi.org/10.1016/j.tws.2020.106682>.
- Dias Martins, A., Camotim, D., and Borges Dinis, P. 2017. “On the direct strength design of cold-formed steel columns failing in local-distortional interactive modes.” *Thin-Walled Structures*, 120, 432–445. <https://doi.org/10.1016/j.tws.2017.06.027>.
- Dinis, P. B., Camotim, D., Landesmann, A., and Martins, A. D. 2020. “Improving the Direct Strength Method prediction of column flexural-torsional failure loads.” *Thin-Walled Structures*, 148, 106461. <https://doi.org/10.1016/j.tws.2019.106461>.
- Dinis, P. B., Camotim, D., Young, B., and Batista, E. M. 2018. “CFS lipped channel columns affected by L-D-G interaction. Part II: Numerical simulations and design considerations.” *Computers & Structures, CIVIL-COMP 2017*, 207, 200–218.
<https://doi.org/10.1016/j.compstruc.2017.03.017>.
- Leng, J., Li, Z., Guest, J. K., and Schafer, B. W. 2014. “Shape optimization of cold-formed steel columns with fabrication and geometric end-use constraints.” *Thin-Walled Structures*, 85, 271–290. <https://doi.org/10.1016/j.tws.2014.08.014>.

- Li, Z., Ádány, S., and Schafer, B. W. 2013. “Modal identification for shell finite element models of thin-walled members in nonlinear collapse analysis.” *Thin-Walled Structures*, 67, 15–24. <https://doi.org/10.1016/j.tws.2013.01.019>.
- Li, Z., Leng, J., Guest, J. K., and Schafer, B. W. 2016. “Two-level optimization for a new family of cold-formed steel lipped channel sections against local and distortional buckling.” *Thin-Walled Structures*, 108, 64–74. <https://doi.org/10.1016/j.tws.2016.07.004>.
- Li, Z., and Schafer, B. W. 2010. “Application of the finite strip method in cold-formed steel member design.” *Journal of Constructional Steel Research*, 66 (8–9), 971–980. <https://doi.org/10.1016/j.jcsr.2010.04.001>.
- Martins, A. D., Camotim, D., and Dinis, P. B. 2018. “On the distortional-global interaction in cold-formed steel columns: Relevance, post-buckling behaviour, strength and DSM design.” *Journal of Constructional Steel Research*, 145, 449–470. <https://doi.org/10.1016/j.jcsr.2018.02.031>.
- Martins, A. D., Dinis, P. B., Camotim, D., and Providência, P. 2015. “On the relevance of local–distortional interaction effects in the behaviour and design of cold-formed steel columns.” *Computers & Structures*, 160, 57–89. <https://doi.org/10.1016/j.compstruc.2015.08.003>.
- Schafer, B. W. 2002. “Local, Distortional, and Euler Buckling of Thin-Walled Columns.” *Journal of Structural Engineering*, 128 (3), 289–299. [https://doi.org/10.1061/\(ASCE\)0733-9445\(2002\)128:3\(289\)](https://doi.org/10.1061/(ASCE)0733-9445(2002)128:3(289)).
- Schafer, B. W. 2008. “Review: The Direct Strength Method of cold-formed steel member design.” *Journal of Constructional Steel Research*, 64 (7–8), 766–778. <https://doi.org/10.1016/j.jcsr.2008.01.022>.
- Schafer, B. W. 2019. “Advances in the Direct Strength Method of cold-formed steel design.” *Thin-Walled Structures*, 140, 533–541. <https://doi.org/10.1016/j.tws.2019.03.001>.
- Schafer, B. W., and Peköz, T. 1998. “Computational modeling of cold-formed steel: characterizing geometric imperfections and residual stresses.” *Journal of Constructional Steel Research*, 47 (3), 193–210. [https://doi.org/10.1016/S0143-974X\(98\)00007-8](https://doi.org/10.1016/S0143-974X(98)00007-8).
- SFIA. 2018. *Technical guide for cold-formed steel framing products*. Steel Framing Industry Association, Falls Church, VA.
- Silvestre, N., Camotim, D., and Dinis, P. B. 2012. “Post-buckling behaviour and direct strength design of lipped channel columns experiencing local/distortional interaction.” *Journal of Constructional Steel Research*, 73, 12–30. <https://doi.org/10.1016/j.jcsr.2012.01.005>.
- Urala, V. 2004. “BRACING REQUIREMENTS OF COLD-FORMED STEEL CEE-STUDS SUBJECTED TO AXIAL COMPRESSION.” Master, University of Florida.
- Vieira, L. C. M., and Schafer, B. W. 2013. “Behavior and Design of Sheathed Cold-Formed Steel Stud Walls under Compression.” *Journal of Structural Engineering*, 139 (5), 772–786. [https://doi.org/10.1061/\(ASCE\)ST.1943-541X.0000731](https://doi.org/10.1061/(ASCE)ST.1943-541X.0000731).
- Xia, Y., Ding, C., Li, Z., Schafer, B. W., and Blum, H. B. 2021. “Numerical modeling of stress-strain relationships for advanced high strength steels.” *Journal of Constructional Steel Research*, 182, 106687. <https://doi.org/10.1016/j.jcsr.2021.106687>.
- Yun, X., and Gardner, L. 2017. “Stress-strain curves for hot-rolled steels.” *Journal of Constructional Steel Research*, 133, 36–46. <https://doi.org/10.1016/j.jcsr.2017.01.024>.
- Zeinoddini, V. M., and Schafer, B. W. 2012. “Simulation of geometric imperfections in cold-formed steel members using spectral representation approach.” *Thin-Walled Structures*, 60, 105–117. <https://doi.org/10.1016/j.tws.2012.07.001>.